RESEARCH PAPER

Evaluation of Simultaneous Effect of Melt Filtration and Cooling Rate on Tensile Properties of A356 Cast Alloy

A. Khakzadshahandashti[1,*], N. Varahram[1], P. Davami[1] and M. Pirmohammadi[2]

**a.khackzad@gmail.com,*

Received: June 2018 **Revised: April 2019** **Accepted: May 2019**

[1] Department of Materials Science and Engineering, Sharif University of Technology, Iran.

[2] Department of Mechanical Engineering, Pardis Branch, Islamic Azad University, Pardis, Iran.

DOI: 10.22068/ijmse.16.2.44

Abstract: *The combined influence of both melt filtration and cooling rate on the microstructure and mechanical properties of A356 cast alloy was studied. A step casting model with five different thicknesses was used to obtain different cooling rates. The effect of melt filtration was studied by using 10 and 20 pores per inch (PPI) ceramic foam filters in the runner. Results showed that secondary dendrite arm spacing decreased from 80 μm to 34 μm with increasing cooling rate. Use of ceramic foam filters in the runner led to the reduction of melt velocity and surface turbulence, which prevented the incorporation of oxide films and air in the melt and consequently had an overall beneficial effect on the quality of the castings. A matrix index, which is the representative of both SDAS and microporosity content, was defined to consider the simultaneous effect of melt filtration and cooling rates on UTS variations. Also, the fracture surface study of test bars cast using 10 and 20 PPI ceramic foam filters showed features associated with ductile fracture.*

Keywords: *Aluminum alloys; microstructure; tensile properties; defects .*

1. INTRODUCTION

Cast A356 aluminum alloy is one of the most well-developed aluminum alloys due to its outstanding properties. It is widely used in numerous automotive and industrial weight-sensitive applications, such as aeronautics and space flights, because of its low density and excellent castability [1]. However, in most cases, superior mechanical properties are required for numerous applications. It has been proven that the strength and hardness of alloys mainly depend on the microstructural features of the solidified part, and can be improved by refining the microstructure. Controlling of casting parameters and addition of chemical modifiers to the melt provide a desirable solidified microstructure [2].

One of the effective casting parameters to control the microstructure of the as-cast alloys is the cooling rate. It is known that as the cooling rate is increased, the microstructural features, especially the grain size and the secondary dendrite arm spacing (SDAS), are decreased. Also, changing the cooling rate can change the porosity percentage and the amounts of the phases present [3]. In addition, the use of filters can also improve the quality of castings. Removing of inclusions from the molten metal is the main effect of a filter, but controlling of the melt flow velocity for the prevention of the turbulent flow is another advantage of using ceramic foam filters in the mold. Turbulent melt flow during casting leads to the formation of a variety of defects such as porosities and oxide films.

There are many papers [4-6] available on the widely used Al-Si-Mg alloys. However, most experimental data often relate the mechanical properties to only one microstructural parameter, such as secondary dendrite arm spacing or solidification defects, and do not take their simultaneous effect into consideration. The aim of the present work was the investigation of the combined influence of the cooling rate and melt filtration on the microstructure, solidification defects and mechanical properties of A356 aluminum alloys. In this regards, a step mold casting with five different thicknesses was used to obtain different cooling rates, and melt filtration was performed using various ceramic foam filters in the runner. Microstructural features and defects amount in

[DOI: 10.22068/ijmse.16.3.44]

A356 castings are strongly dependent on different cooling rates. On the other hand, melt filtration controls the amount of defects such as microporosity and oxide bifilms in A356 castings, so a matrix index, which was the representative of both microstructural features and defects content, was defined to consider the simultaneous effect of cooling rates and melt filtration.

2. EXPERIMENTAL PROCEDURE

2.1. Materials and casting process

The schematic view and geometry of the casting with five steps are shown in Fig. 1. The total width and length of the mold are 150 mm and 287.50 mm, respectively. In addition, the thickness and width of each step are 5.80 mm and 51.50 mm, respectively. This configuration allowed a range of cooling rates and consequently resulted in different microstructures in the castings. To study the effect of melt filtration, castings were conducted with and without ceramic foam filters in the runner.

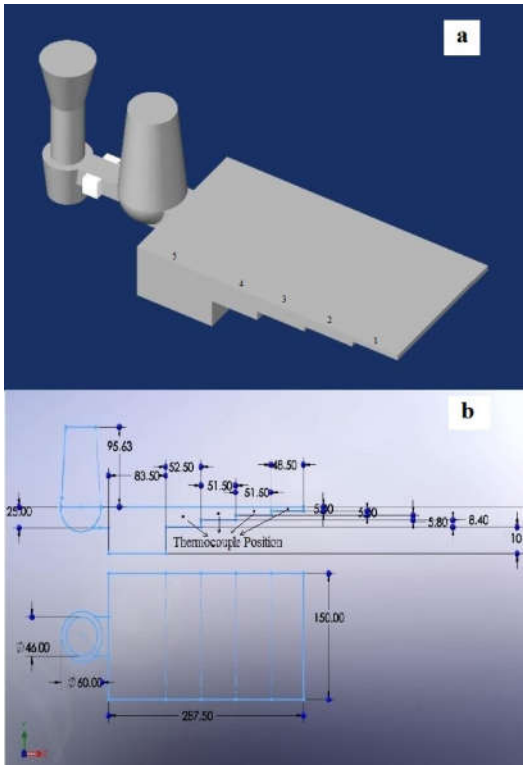

Fig. 1. (a) Schematic illustration, and (b) dimensions of the mold (in mm).

The material used in this study was commercial cast A356 aluminum alloy. A cylindrical sample with the diameters of 20 millimeters and height of 10 millimeters was cut from the end of A356 billets. The chemical composition of the alloy was measured by an optical emission spectroscopy. The alloy ingot was melted in an electrical resistance furnace and degassed using argon degassing ceramic lance for 5 mins. To modify the microstructure, 0.03 wt. % strontium was added into the melt. The melt was then poured into the sand mold at 720 °C. The temperature was measured using K-type thermocouples covered with ceramic sheaths inserted at each step of casting. These thermocouples were connected to a data acquisition system and a computer, to record the time-temperature data. The solidification time was calculated between the liquidus and eutectic temperatures. In order to ensure statistical accuracy, the casting was repeated three times for each step.

2.2. Microstructural analysis

The thermocouples were removed and specimens were cut out from the sections where the tips of the thermocouples were located from solidified castings. For metallographic observation, the specimens were ground, polished and etched in 0.5% Hydrofluoric acid and then observed with an optical microscope. In order to measure the secondary dendrite arm spacing (SDAS) of primary α-aluminum phase, image analysis was performed on 9 optical micrographs for each specimen. The fracture surfaces of tensile test bars were examined with a scanning electron microscope (SEM) and chemical analyses of these surfaces were performed with the X-ray energy dispersive spectroscopy (EDS) analyzer linked to the SEM microscope.

2.3. Tensile testing

Tensile tests were carried out on a SANTAM STM-150 machine, at room temperature and at a nominal strain rate of 3.9 ×10-4 s-1, using flat specimens, with a gauge length of 25 mm. To ensure reproducibility of the tensile results, three specimens were tested for each step.

[DOI: 10.22068/ijmse.16.3.44]

2.4. Volumetric porosity and melt velocity calculation

The volumetric porosity was calculated using the Archimedes' method. It is noteworthy to say that, the theoretical density of the water which is dependent on room temperature could be the source of errors in porosity calculation. In addition, the buoyancy effect of water infiltration into surface-breaking pores is another source of errors. Also, the melt velocity in the runner was measured using the SutCast software.

3. RESULTS AND DISCUSSION

3.1. Microstructural characterization

The chemical composition of the alloy is shown in Table 1. Fig. 2 indicates the microstructure of A356 alloy at different steps of the casting. All microstructures consisted of primary α-Al dendrites (light regions) and eutectic silicon particles (dark regions) in the interdendritic regions. The coarser dendrite arms of α-Al of specimens cut from the thicker steps (i.e. slower cooling rates) were the main difference of microstructures. It is

Table 1. Exact chemical composition of the experimented alloy

Si	Mg	Fe	Ti	Cu	Ni	Zn	Sn	Mn	Al
7.25	0.44	0.2	0.01	0.14	0.005	0.04	<0.005	0.02	Balance

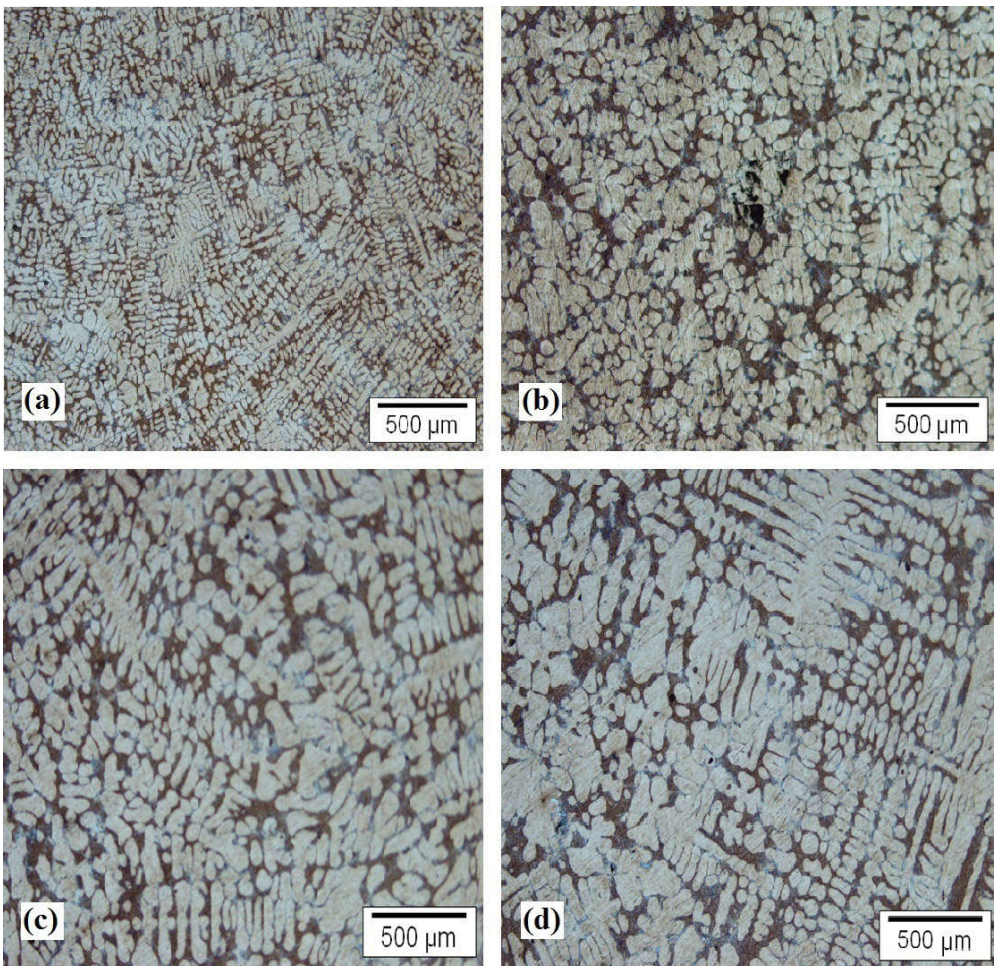

Fig. 2. Microstructure of castings at solidification times of: (a) 34 s, (b) 47 s, (c) 49 s and (d) 51 s.

[DOI: 10.22068/ijmse.16.3.44]

well known that a high cooling rate and a short solidification time lead to the formation of a more refined microstructure which significantly affects the mechanical properties [7].

Fig. 3 shows the variation of SDAS versus local solidification time. It can be observed that SDAS increases due to the decrease in cooling rate (i.e. the increase of solidification time). This figure also shows a comparison between the SDAS experimental values and those calculated by Kurz [7] and Bamberger [8] approaches. The Kurz and Fisher approach was expressed by Eq. (1).

$$SDAS = 5.5(Mt_{Sl})^{\frac{1}{3}} \quad [1]$$

$$M = -\frac{\Gamma D_L}{(1-k_0)m_L(C_E - C_0)}\ln(\frac{C_E}{C_0}) \quad [2]$$

In Eq. 1, t_{Sl} is the solidification time, and M is a parameter which is defined by Eq. 2. In Eq. 2, Γ is the Gibbs-Thomson coefficient, D_L the solute chemical diffusivity in the liquid, k_0 the partition coefficient, C_0 the alloy composition, C_E the eutectic composition, and m_L is the liquidus slope in the Kurz and Fisher model. Bamberger's model was expressed by Eq. (3).

$$SDAS = A_{Si}(t_{Sl})^{0.43} \quad [3]$$

Where ASi is a constant which varies inversely with the silicon content in the Bamberger's model; ASi=12.8 for A356 alloy [8]. The solidification times were obtained from results of thermocouples and the data acquisition system, so the values of SDAS measured in the microstructure analyses were compared to the values calculated from these two models. The SDAS experimental results were lower than values predicted by Bamberger's model, but these values are in a good agreement with the Kurz and Fisher model.

The quantitative relationships between volumetric porosity percentage and SDAS for different experimental situations are shown in Fig. 4. Obviously, the microporosity content decreases with the decrease of the SDAS. During the last stages of the solidification process, feeding the interdendritic regions of the melt becomes difficult, so shrinkage porosities can form in the isolated areas [2]. With the decrease of SDAS at high cooling rates, the volumetric porosity content decreased due to the reduction of interdendritic regions and space constriction. It is noticeable that with slower cooling rate, the volumetric porosity increased by 40.3 %, 40.6 %, and 44.1 % for castings made without and with 10 PPI and 20 PPI ceramic foam filters, respectively. The melt filtration using ceramic foam filters leads to a decrement in the volumetric porosity percentage.

The main causes of porosity formation in the A356 casting alloy are both volumetric shrinkage and dissolved hydrogen gas [2]. As reported by Anson and Gruzleski [9], the formation of shrinkage porosity is due to a difference of density be-

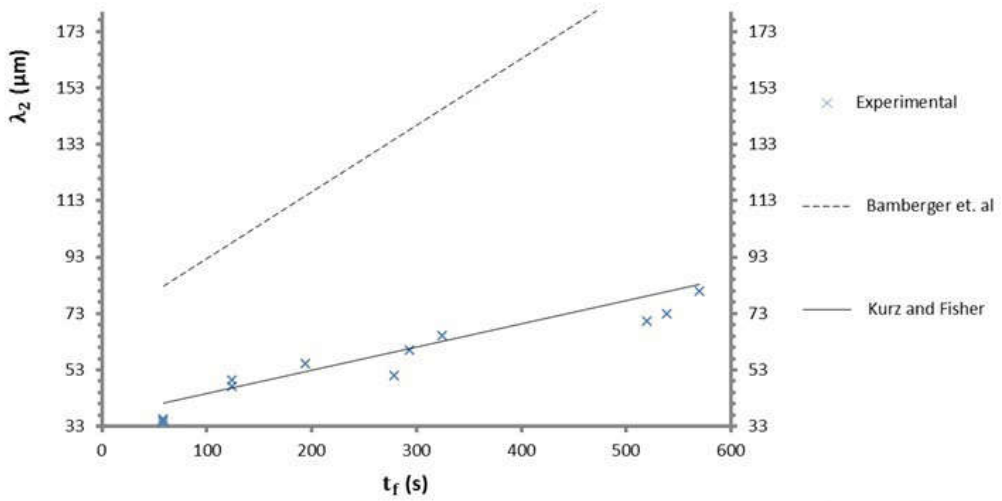

Fig. 3. Secondary dendrite arm spacing as a function of solidification time.

[DOI: 10.22068/ijmse.16.3.44]

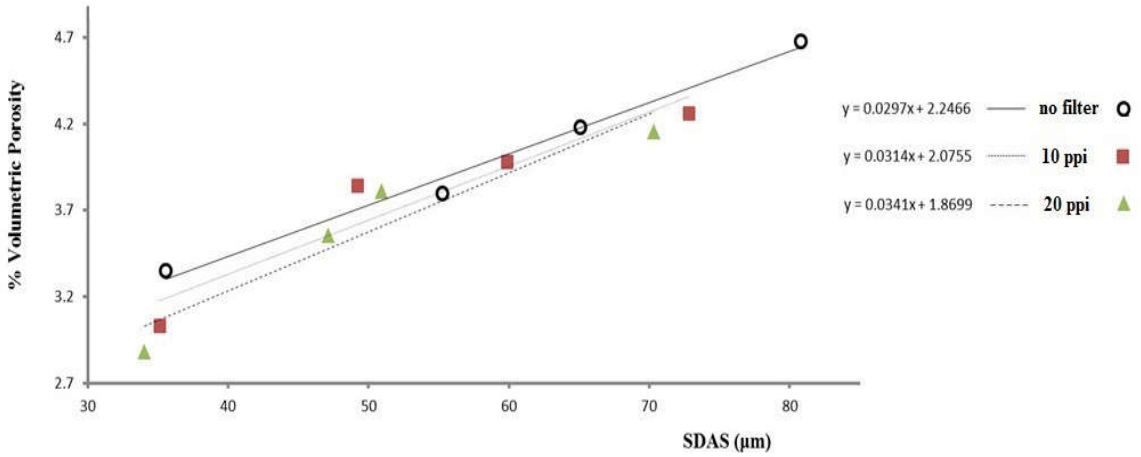

Fig. 4. Variations of volumetric porosity versus secondary dendrite arm spacing.

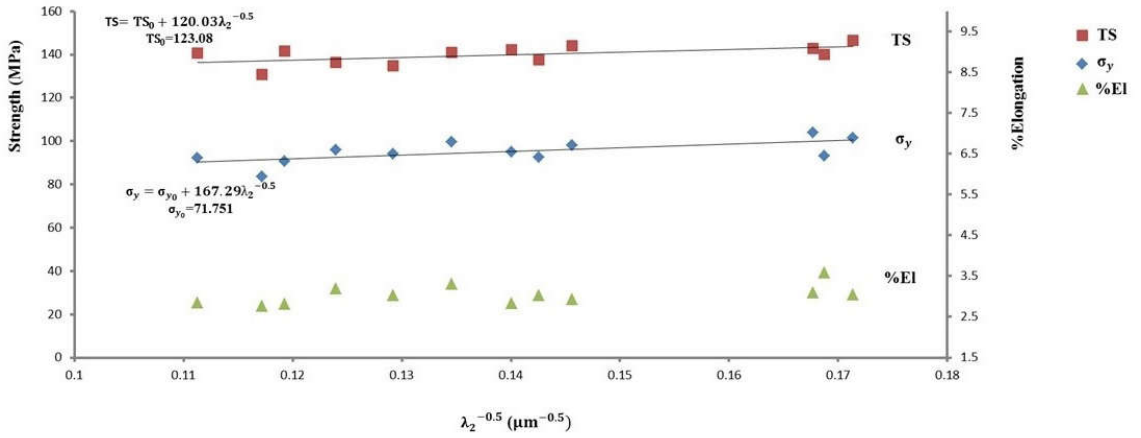

Fig. 5. Effect of secondary dendrite arm spacing on mechanical properties.

tween the liquid and solid phases. Gas porosities also form because of the low solubility of hydrogen in the solid-state raher than the liquid [10]. Also, the main source of hydrogen gas is water vapor in the air. Design of unsuitable running systems can lead to turbulence in the melt and the higher amounts of air in the melt [11]. As reported by Campbell [2], control of the melt velocity at the range of 350 mm/s to 500 mm/s is necessary to eliminate turbulence of the molten aluminum. An effective way for control of the melt velocity is the use of a filter in the runners. In this study, the value of melt velocity in the runner was obtained from a melt flow simulation by the SutCast software. The melt velocity in the castings with 10 PPI and 20 PPI ceramic foam filters was 430 mm/s and 580 mm/s, respectively, while the melt velocity in the casting without a filter was 1840 mm/s [12]. Therefore, melt filtration showed a reduction of the amount of dissolved hydrogen gas and volumetric porosity due to a decrease in the turbulence of the melt.

3.2. Tensile Properties

Fig. 5 presents the experimental results of yield strength (0.2 % proof strength, σy), elongation, and ultimate tensile strength (σUTS) as a function of SDAS. It can be seen that mechanical properties increase with the decrease of SDAS values. The results are consistent with other works on Al-Si commercial as-cast alloys [3-5, 13].

[DOI: 10.22068/ijmse.16.3.44]

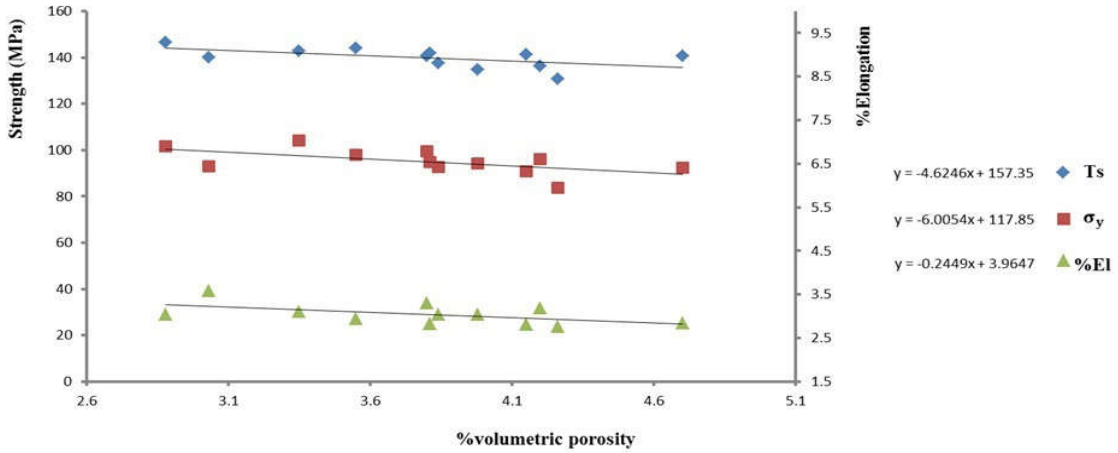

Fig. 6. Effect of volumetric porosity on mechanical properties

Fig. 6 illustrates the variations of mechanical properties versus volumetric porosity. As shown in this figure, the yield, ultimate tensile strength, and elongation of the A356 alloy exhibit an obviously linear dependence on the variation of volumetric porosity. According to Osorio et al. [4], the improvement in tensile properties cannot be attributed only to smaller dendritic spacings and it seems to be the result of a number of separate effects. For instance, a combination of a more homogeneous distribution of the eutectic mixture for smaller spacings and reduction in porosity and double oxide films improve the mechanical properties.

3.3. Relationship between tensile strength and matrix index

Different cooling rates significantly affect SDAS and microporosity content and melt filtration controls microporosity content in A356 castings. A matrix index, which was the representative of both SDAS and volumetric porosity, was defined as Eq. 4 to consider the simultaneous effect of cooling rates and melt filtration.

$$M.I. = 97\mathrm{Ln}Vp(\%) + 2\mathrm{Ln}SDAS(\mu m) \quad [4]$$

Volumetric porosity and SDAS values of different trials were used to calculate the matrix index of experimented samples. Fig. 7 shows the relation of the ultimate tensile strength of test bars and matrix index according to Eq. 4. There is a relationship between the matrix index and the ultimate tensile strength values of the examined samples according to Fig. 7. Equation 5 could then had used for the prediction of UTS values in the present work.

$$UTS = -0.355M.I. + 187.71 \quad [5]$$

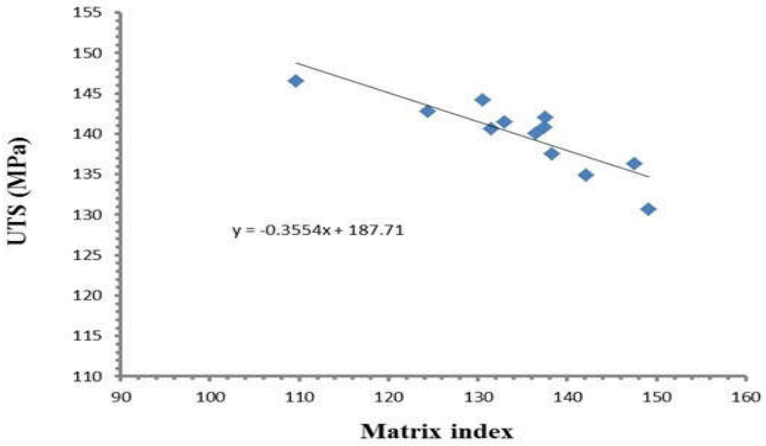

Fig. 7. Ultimate tensile strength as a function of the matrix index.

[DOI: 10.22068/ijmse.16.3.44]

3.4. Fractographic study

The fracture surfaces of the test bars cast without using any filter in the runner showed a considerable amount of oxide film content [12]. Fig. 8.a shows a pore in the fracture surface of the specimen cast with a 10 PPI ceramic foam filter. There is no large oxygen peak in Fig. 8b, so there was no evidence of old oxide films or oxide bifilms incorporated in this pore. The fractographic examination revealed that the oxide bifilms content in the fracture surface of specimens cast with the 20 PPI filter was much lower than specimens cast with the 10 PPI filter or cast without any filter. The fracture surface of the test bars made from sample cast using a ceramic foam filter in the runner showed ductile fracture (Fig. 8c). Results of EDS analyses (Fig. 8d) showed that there was no evidence of oxide films presence in the fracture surface of test specimens, so there was metal-to-metal contact prior to fracture. The presence of dimples on the test bar's fracture surfaces is the evidence of ductile fracture.

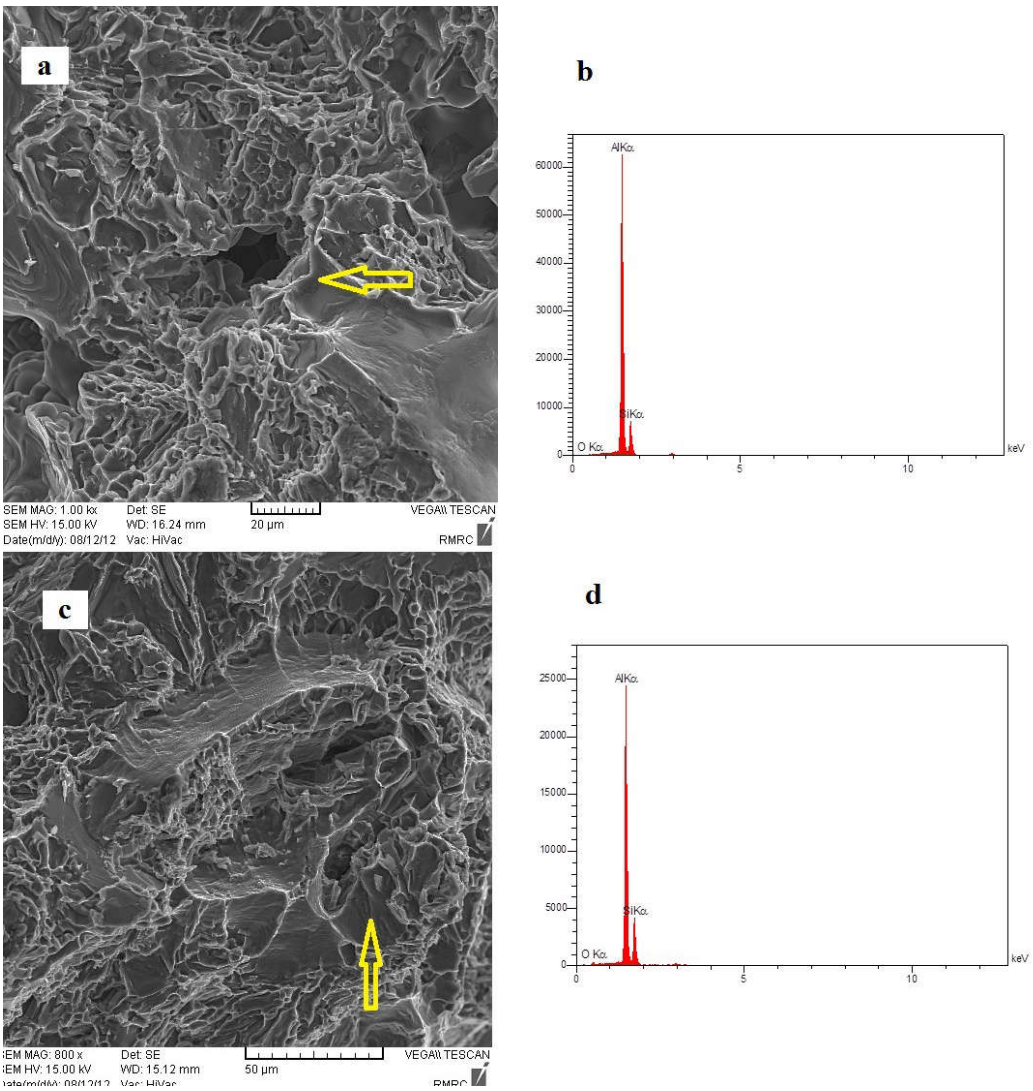

Fig. 8. SEM fractographs of A356 tensile test bars a) fracture surface of the specimen cast with a 10 PPI ceramic foam filter b) EDS analysis of the location shown in (a) c) ductile fracture observed on the fracture surface of the specimen cast with a 20 PPI ceramic foam filter d) EDS analysis of the location shown in (c)

[DOI: 10.22068/ijmse.16.3.44]

4. CONCLUSIONS

In this study, the effects of melt filtration and cooling rate on the microstructure and tensile properties of cast A356 alloy were investigated. The following conclusions can be made from the results of the present investigation:

1. A combination of high cooling rate and melt filtration had an overall beneficial effect on the quality of the castings.
2. With increasing cooling rate, the secondary dendrite arm spacing decreased. The volumetric porosity also decreased due to the space constriction.
3. Use of filters in the runner led to the reduction of melt velocity and surface turbulence, which reduced porosity and dissolved hydrogen gas.
4. The mechanical properties decreased with increasing secondary dendrite arm spacing and volumetric porosity.

REFERENCES

1. Zhang, L.Y., et al., Mechanical properties of cast A356 alloy, solidified at cooling rates enhanced by phase transition of a cooling medium,Mater. Sci. Eng., A ,2007, 448, 361-365.
2. Campbell, J., Invisible macrodefects in castings. J. Phys. IV, 1993, 03, C7-861-C7-872.
3. Dutta, B. and M. Rettenmayr, Effect of cooling rate on the solidification behaviour of Al–Fe–Si alloys. Mater. Sci. Eng., A, 2000, 283, 218-224.
4. Osorio, W.R., et al., Effect of dendritic arm spacing on mechanical properties and corrosion resistance of Al 9 Wt Pct Si and Zn 27 Wt Pct Al alloys. Metall, Mater. Trans. A, 2006, 37, 2525-2538.
5. Goulart, P.R., et al., Mechanical properties as a function of microstructure and solidification thermal variables of Al–Si castings. Mater. Sci. Eng., A, 2006, 421, 245-253.
6. Lee, C.D., Effects of microporosity on tensile properties of A356 aluminum alloy. Mater. Sci. Eng., A, 2007, 464, 249-254.
7. Kurz, W. and D.J. Fisher, Fundamentals of solidification, Trans Tech Publications, 1986.
8. Bamberger, M., B.Z. Weiss, and M.M. Stupel, Heat flow and dendritic arm spacing in chill-cast Al–Si alloys, J. Mater. Sci. Technol., 1987, 3, 49-56.
9. Anson, J.P. and J.E. Gruzleski, The Quantitative Discrimination between Shrinkage and Gas Microporosity in Cast Aluminum Alloys Using Spatial Data Analysis. Mater. Charact., 1999, 43, 319-335.
10. Atwood, R.C., S. Sridhar, and P.D. Lee, Equations for nucleation of hydrogen gas pores during solidification of aluminium seven weight percent silicon alloy. Scripta Mater., 1999, 1255-1259.
11. Weigel, J. and E. Fromm, Determination of hydrogen absorption and desorption processes in aluminum melts by continuous hydrogen activity measurements. Metall. Trans. B, 1990, 21, 855-860.
12. A. Khakzadshahandashti, N.Varahram, and P. Davami, EFFECT OF CERAMIC FOAM FILTERS ON OXIDES REMOVAL AND THE TENSILE PROPERTIES OF A-356 ALLOY CASTINGS. Iranian Journal of Materials Science & Engineering, 2014, 11, 14-24.
13. Zhang, L.Y., et al., Effect of cooling rate on solidified microstructure and mechanical properties of aluminium-A356 alloy. J. Mater. Process. Technol., 2008, 207, 107-111.

[DOI: 10.22068/ijmse.16.3.44]